第 50 卷 第 14 期/2023 年 7 月/中国激光 研究论文

中国激光

轴向张力作用下 As_2S_3 硫系光纤的光敏性及其在 Bragg 光栅刻写方面的应用

邹林儿*，尚磊，杨熙飞，沈云

南昌大学物理与材料学院，江西 南昌 330031

摘要 为进一步提高硫系光纤的光敏性，基于光纤法布里-珀罗标准具原理研究了 As_2S_3 硫系光纤在轴向张力作用下的光敏性，结果表明施加轴向张力能显著提高其光敏性。与未施加轴向压力相比，在第一快过程中，光致折射率负变化幅度减小，经历的时间可缩短至数十秒；在第二慢过程中，光致折射率变化 Δn 加快朝正方向恢复，在一定张力作用下光致折射率变化 Δn 出现正增长，Δn 增长幅度可达到 5.41×10^{-3}。基于这一显著光敏性刻写了 As_2S_3 硫系光纤 Bragg 光栅，在 70～110 s 的短曝光时间内，光栅透射深度平均值达到了 9.46 dB，且光栅光谱质量良好。本研究为制备高反射率硫系光纤光栅提供了新思路和新途径。

关键词 光纤光学；硫系玻璃光纤；张力；光敏性；光纤光栅

中图分类号 TN253 **文献标志码** A **DOI**：10.3788/CJL230438

1 引 言

以硫系玻璃为基质材料的硫系光纤近年来发展迅速，已成为当前国际上光子功能器件研究和开发的前沿和热点之一[1-3]。硫系玻璃是以硫族元素 S、Se、Te 为基质，结合 As、Sb、Ge、Ga 等元素制成的硫系基质材料，具有高的折射率（2.0～3.5）、极高的非线性系数（石英材料的 10^2～10^3 倍）、超快的非线性响应（响应时间小于 200 fs）、优良的中远红外透光性（在 0.4～22 μm 波段存在宽广的红外透射窗口），在光通信波段具有非常低的双光子吸收且不存在自由载流子吸收等优良的光学特性[4-7]，是一种新型的红外光子器件基质材料。其中的 As-S 玻璃体系因具有较为稳定的化学性能而被国内外广泛研究。硫系玻璃光纤 Bragg 光栅是应用非常广泛且非常重要的硫系光子器件之一，作为线性器件，它可应用于红外传感器[8-9]；在非线性光学应用中，它可以实现全光信号处理[10-13]。同时，在高效一体硫系玻璃光纤激光器特别是分布式反馈布里渊激光器中，具有高反射率的 Bragg 光栅尤其重要[14-16]。对于基于硫系玻璃体材料或薄膜材料的体光栅[17-19]，可基于其在光诱导下折射率随光照时间延长而增大并达到饱和状态这一光敏现象进行刻写[20-22]；而对于硫系玻璃光纤光栅的刻写，情况则更为复杂，主要是因为硫系玻璃光纤包层和纤芯的组分类似，两者都有光敏性。本课题组在前期的研究工作中发现，选择靠近材料吸收边缘的近带隙光照射硫系玻璃光纤，纤芯会呈现出较高的光敏性[23-24]，解决了采用远离材料吸收边缘的亚带隙光照射所带来的弱光敏性问题[25-26]。应用传统技术刻写的 Bragg 光栅的透射峰值较小，导致光栅反射率达不到实际使用要求，因而需要采用一定的方法进一步提高硫系光纤的光敏性。文献[27-28]指出，在光纤上施加轴向张力可对光纤的光敏性产生一定影响，对锗硅光纤施加外部应变可以增强 193 nm 处的光敏性，掺铒光纤在张力作用下的光敏性会降低。基于此，笔者通过实验详细探究了沿轴向施加张力条件下硫系光纤的光敏性，结果显示施加张力能显著提高硫系光纤的光敏性。基于此研究结果，笔者刻写了硫系光纤 Bragg 光栅，获得了高达 89.7% 的光栅反射率。

2 实验装置与原理

图 1(a)是基于法布里-珀罗（FP）标准具原理测量纤芯折射率变化的实验装置图[23]。该实验装置中带滑块的光纤夹具由本课题组自行设计，光纤一端固定在夹具的固定点上，另一端固定在夹具的滑块上，通过悬挂砝码或拉伸弹簧测力计施加张力推动滑块，然后拧紧螺母固定滑块，使光纤受到一定的轴向张力。改变砝码重量可以定量地改变光纤的轴向张力。实验中使用的是连续双频 Nd:YAG 激光器，选用工作波长为 532 nm 激光作为照射光源。光束经扩束系统扩束后，通过柱面透镜聚焦在样品表面上，形成高度约为 1.1 mm、

收稿日期：2023-01-05；**修回日期**：2023-02-10；**录用日期**：2023-02-27；**网络首发日期**：2023-03-09

基金项目：国家自然科学基金（62165008，61465008）、江西省自然科学基金（20212ACB201007）

通信作者：*linerzou@ncu.edu.cn

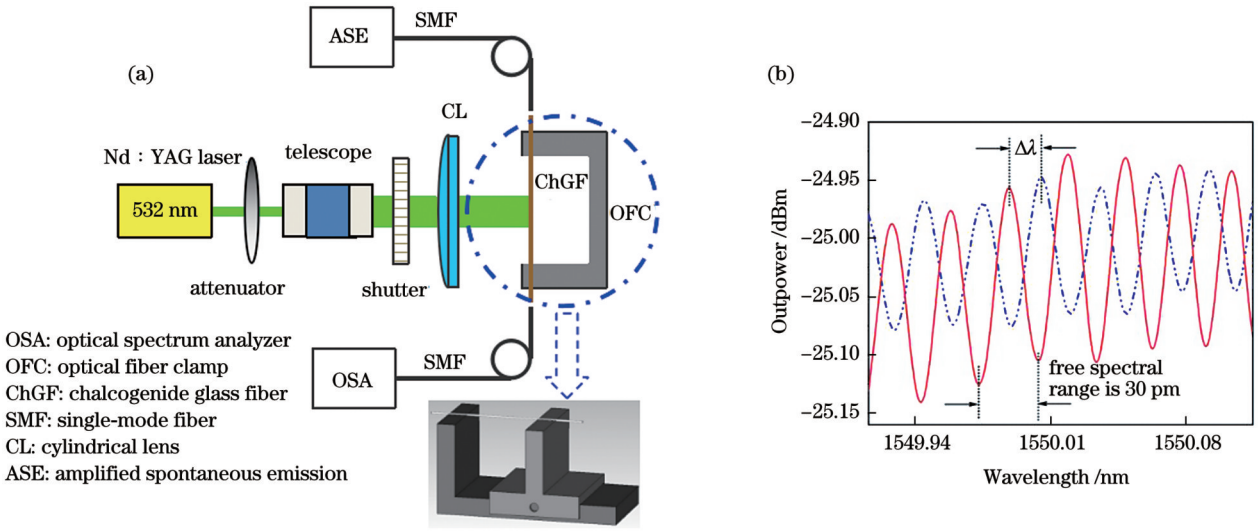

图 1 实验装置与测量原理。(a)沿轴向施加张力测量硫系光纤的光致折射率变化的实验装置示意图;(b)光照射硫系光纤时 OSA 测得的波形图位移,由此可计算出光致折射率变化

Fig. 1 Experimental setup and measuring principle. (a) Schematic of experimental setup for measuring the photorefractive index change of chalcogenide optical fiber by applying tension along the axial direction; (b) displacement of oscillogram measured by OSA when light irradiates chalcogenide optical fiber for calculating the photorefractive index change

宽度约为 5 mm 的强度呈高斯分布的光斑。光照时间由电子快门控制(控制范围为 0.001~999.999 s),光照功率通过可变衰减器改变。选用纤芯/包层直径约为(8±1) μm/(170±8) μm、损耗约为 0.1 dB/m@1550 nm 的低损耗商业化 As_2S_3 光纤,纤芯和包层对应的组分分别为 $As_{39}S_{61}$ 和 $As_{38}S_{62}$,两者的折射率差异约为 0.3%,纤芯折射率约为 2.415。利用超声波切割刀切割 As_2S_3 光纤,制作一个两端面光滑且平行、长约为 15 mm 的 FP 标准具。采用线性偏振、带宽为 1520~1570 nm 的放大自发辐射光源(ASE)作为测量信号光束,该光束通过单模光纤端面耦合到 FP 标准具并在 FP 标准具内发生多次镜面反射,得到的干涉波形图用高分辨率光谱分析仪(OSA)进行监测。如图 1(b)所示,只需在 FP 标准具上引入微小的光程差,干涉波形就会发生位移 Δλ,通过 OSA 测量 Δλ 就可以计算得到纤芯的光致折射率变化 Δn[23]。计算公式为

$$\Delta n = n \cdot \frac{\Delta\lambda}{\lambda} \cdot \frac{L}{l}, \tag{1}$$

式中:n 是硫系光纤纤芯折射率;L 是 FP 标准具的长度;l 是光照射在光纤上的长度;λ 是测得的中心波长。在该实验中,$n=2.415$,$L=15$ mm,$l=5$ mm,$\lambda=1550$ nm。

3 轴向张力作用下 As_2S_3 光纤的光敏性

3.1 相同张力不同光照功率下的光致折射率变化

实验中使用的光纤是在同一根光纤上截取的,以保证实验结果的准确性与一致性。图 2(a)、(b)分别是光照功率为 10 mW 情况下未施加张力和施加张力时 As_2S_3 光纤芯层光致折射率变化与光照时间的关系。图 2(a)显示:未施加张力时,在第一快过程中,光致折射率变化 Δn 减小到约 -1.78×10^{-3},经历的时间为 340 s;之后随着光照时间延长,出现第二慢过程,光致

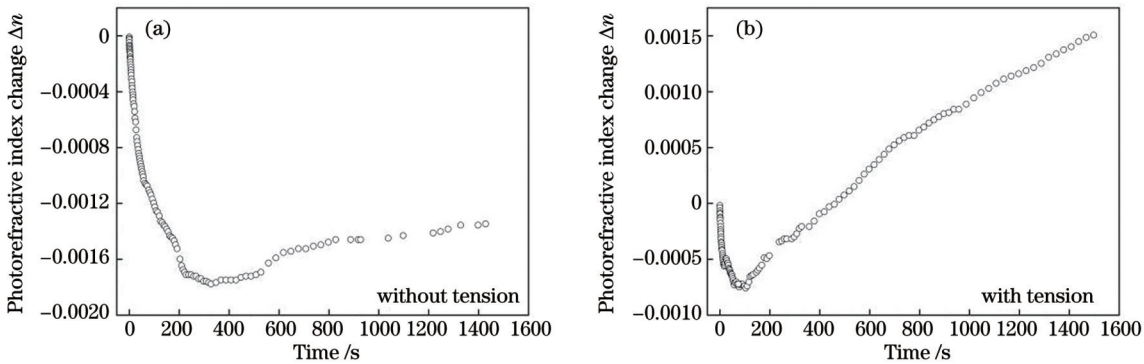

图 2 在光照功率为 10 mW 时,As_2S_3 光纤芯层光致折射率变化 Δn 与光照时间的关系。(a)没有施加张力;(b)施加 0.490 N 张力

Fig. 2 Dependence of the photorefractive index change Δn of As_2S_3 fiber core on the illumination time under the light irradiation power of 10 mW. (a) Without tension; (b) with tension of 0.490 N

折射率缓慢恢复，在光照时间为1400 s时，光致折射率变化Δn恢复到约-1.37×10^{-3}。当在样品上施加0.490 N张力时，光致折射率变化Δn与光照时间的关系如图2(b)所示，可见：在第一快过程中，光致折射率变化Δn减小到约-7.57×10^{-4}，经历的时间缩短为110 s；在第二慢过程中，光致折射率快速恢复，且在光照时间为460 s时光致折射率出现了正方向增长，在光照时间为1500 s时，光致折射率变化Δn可达到1.51×10^{-3}。

在光照功率增加情况下研究了相同大小的张力对光敏性的影响。图3(a)、(b)分别是在光照功率提高到13 mW情况下，未施加张力和施加张力时As_2S_3光纤芯层光致折射率变化Δn与光照时间的关系。图3(a)显示：在较高的光照功率下，没有施加张力时，第一快过程的光致折射率变化Δn快速减小到约为-8.51×10^{-4}，经历的时间为120 s(与10 mW光照功率下相比缩短了220 s)；在第二个光致折射率恢复的慢过程中，随着光照时间增加，折射率缓慢恢复，在光照时间为1600 s时光致折射率恢复幅度约为-2.37×10^{-4}。当在样品上施加0.490 N张力时，光致折射率变化Δn随光照时间的变化如图3(b)所示，可见：在较高的光照功率下，第一快过程的光致折射率负变化幅度约为-6.44×10^{-4}，经历的时间显著缩短，为27 s；在折射率恢复的第二慢过程中，只需128 s光照光致折射率变化Δn就出现了正增长，在光照时间为1700 s时，光致折射率增加幅度约为5.41×10^{-3}。

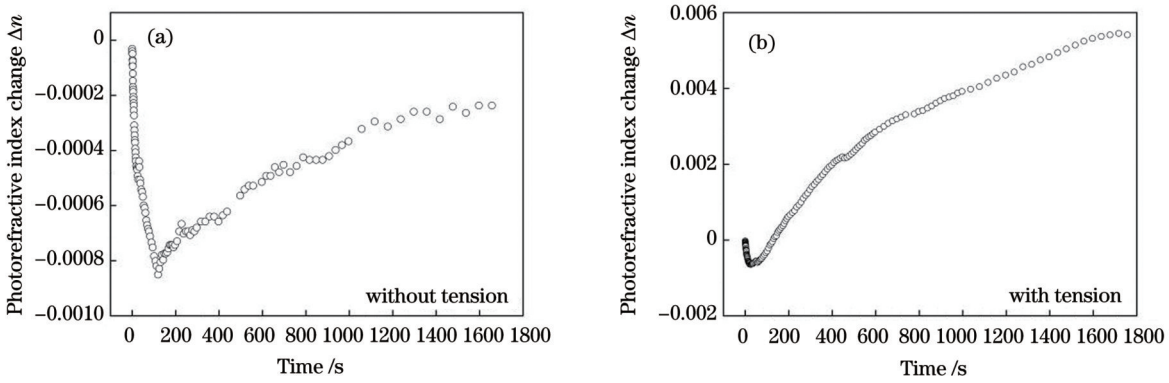

图3　光照功率为13 mW时，As_2S_3光纤芯层光致折射率变化Δn与光照时间的关系。(a)没有施加张力；(b)施加0.490 N张力

Fig. 3　Dependence of the photorefractive index change Δn of As_2S_3 fiber core on the illumination time under the light irradiation power of 13 mW. (a) Without tension; (b) with tension of 0.490 N

由图2和图3的分析可知，施加轴向张力能显著提高As_2S_3硫系光纤的光敏性。施加张力后，第一快过程的光致折射率负变化幅度减小，经历的时间明显缩短；在第二慢过程中，光致折射率随着光照时间延长缓慢恢复，并在一定张力下出现正增长，变化幅度可达到10^{-3}量级。另外，图2(b)和图3(b)显示：在同样的张力作用下，随着光照功率增加，光致折射率变化Δn的第一快过程明显缩短，可缩短至数十秒；在第二慢过程中折射率恢复加快，且光致折射率出现正增长的幅度更大，高达5.41×10^{-3}。

3.2　不同张力相同光照功率下的光致折射率变化

本文还研究了相同光照功率下不同张力对光敏性的影响。图4(a)、(b)是光照功率为11 mW情况下分别施加0.274、0.353 N张力时As_2S_3光纤光致折射率变化Δn与光照时间的关系。图4(a)显示：在较小的0.274 N张力作用下，第一快过程的光致折射率变化Δn减小至

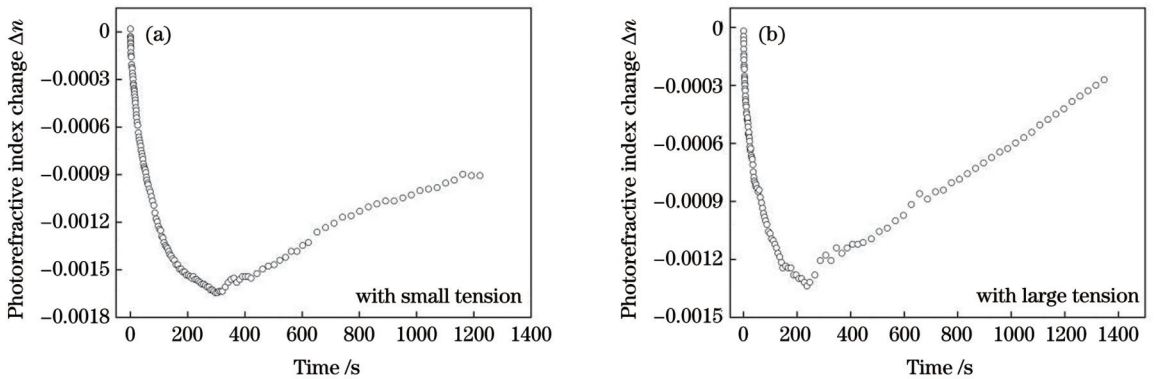

图4　光照功率为11 mW时，As_2S_3光纤芯层折射率变化Δn与光照时间的关系。(a)施加0.274 N张力；(b)施加0.353 N张力

Fig. 4　Dependence of the photorefractive index change Δn of As_2S_3 fiber core on the illumination time under the light irradiation power of 11 mW. (a) With tension of 0.274 N; (b) with tension of 0.353 N

约-1.65×10^{-3}，经历的时间为300 s；在第二慢恢复过程中，折射率缓慢恢复，在光照时间为1200 s时光致折射率变化Δn恢复到约为-9.06×10^{-4}。当增大张力至0.353 N时，光致折射率变化Δn与光照时间的关系如图4(b)所示，可见：在第一快过程中，光致折射率负变化幅度减小到-1.34×10^{-3}左右，经历的时间缩短至230 s；在第二慢过程中，折射率缓慢恢复，在光照时间为1300 s时光致折射率变化Δn恢复到约-2.99×10^{-4}。

上述分析表明，在同样大小的光照功率下，随着施加的轴向张力增大，光致折射率变化Δn的第一快过程经历的时间明显缩短，且折射率负变化幅度减小；在第二慢过程中，较大的张力可加快折射率恢复。

研究人员在研究硫系玻璃薄膜光黑化现象过程中，也观察到了类似光诱导下出现的两种行为[29]。Abduhalim等[29-30]提出了光诱导动力模型，认为：第一快过程的产生源于缺陷态，其持续的时间τ_G与光照强度I的关系为$\tau_G\propto1/I$；缺陷态处于亚稳定状态，进入第二慢过程会使其稳定化，稳定过程的持续时间τ_S取决于产生的缺陷数量，最终饱和态的折射率增加幅度Δn正比于$I^{2/3}$。综合文献[27-28,31]可知，目前尚没有特定的理论针对沿轴向施加的张力与光纤光敏性之间的关系进行分析。实际上，在沿轴向拉伸光纤时，光纤横向(径向)会存在压缩力，且在光照射的部分该力能更有效地压缩光纤；停止光照后，压缩状态将持续。沿光纤径向施加作用力也可获得该横向压缩力，可为后续研究硫系光纤用于径向压力传感器提供参考。基于此事实，进而考虑当硫系光纤处于这种应力状态时，可采用带干涉条纹图案的光从侧面照射光纤，在光纤中形成一种压实图案，使得压实区域具有更高的折射率，由此产生折射率图案，形成光纤光栅。

4 刻写Bragg光栅

采用Nd:YAG激光器(选用波长为532 nm的曝光光源，其光功率为300 mW)和带+1/−1衍射级的相位掩模板搭建改进型Sagnac干涉系统[24]，通过它形成干涉条纹图案，用于刻写光纤Bragg光栅。在该系统中，优化Sagnac干涉系统的光路系统，使两高斯光斑具有更好的重合效果，以便得到对比度更高的干涉条纹。在实验中，测得+1/−1衍射级每束光的强度约为3 mW，两光束夹角2θ约为110.67°，光栅周期Λ约为323.39 nm，在光纤样品上形成了宽约为7.2 mm、高约为1.1 mm的干涉图形。数值孔径为0.24的原As_2S_3硫系玻璃光纤在波长1550 nm处的归一化频率约为3.4，存在多个模式。要满足单模，其归一化频率应小于2.4，对应的纤芯直径应小于4.9 μm。为得到单模，采用热熔融拉锥技术将商业化原As_2S_3硫系玻璃光纤拉锥为纤芯/包层直径分别约为4.3 μm/92.3 μm的小直径光纤。图5(a)、(b)是该小直径光纤未通光和通光时的端面照片，图5(b)显示通光时该小直径光纤在波长1550 nm处的光场分布呈单模。

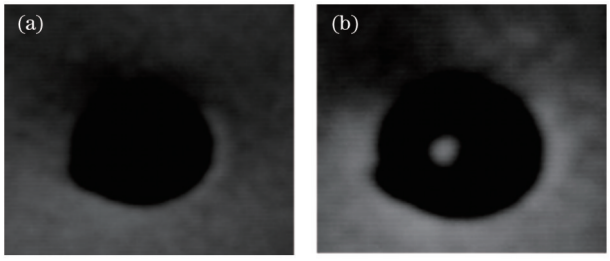

图5 拉锥形成的小直径As_2S_3玻璃光纤端面照片。(a)未通光；(b)通光(端面耦合，中心波长为1550 nm)

Fig. 5 End face photos of tapered As_2S_3 glass fiber with small diameter. (a) Without coupling light; (b) with coupling light (end coupling, the central wavelength of 1550 nm)

笔者通过实验详细考察了在小直径光纤样品上施加0.196 N张力刻写的Bragg光栅的动态特性，并将其与未施加张力时的进行了对照。图6(a)是未施加张力时Bragg透射峰深度与曝光时间的关系，最大透射峰深度值是在曝光时间约为80 s时获得的。图6(b)是未施加张力且曝光时间为80 s的Bragg光栅的透射谱，透射峰深度值约为6.65 dB，反射率约为78%。

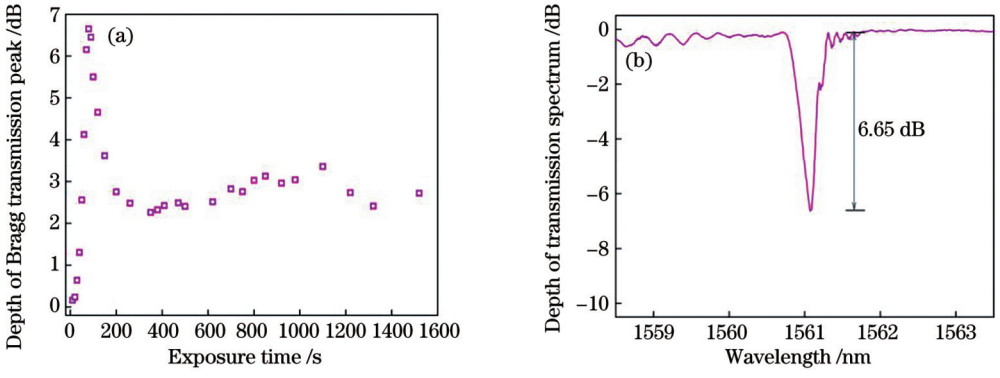

图6 未施加张力刻写的Bragg光栅的特性。(a)Bragg透射峰深度与曝光时间的关系；(b)曝光时间为80 s的Bragg光栅的透射光谱

Fig. 6 Characterization of written Bragg grating without tension. (a) Dependence of the depth of Bragg transmission peak on exposure time; (b) transmission spectrum of Bragg grating with exposure time of 80 s

图 7(a)是施加 0.196 N 张力的 Bragg 透射峰深度与曝光时间的关系，结果显示：在 70～110 s 曝光时间内，中心波长的平均峰值约为 9.46 dB，平均反射率高达 88.6%，而且该时间内的光谱质量良好。图 7(b)是施加 0.196 N 张力并在最佳曝光时间 80 s 时获得的 Bragg 光栅透射谱，结果显示：当施加 0.196 N 张力后，Bragg 光栅透射峰深度值达到了 9.85 dB，反射率提高到 89.7%，光栅带宽约为 0.48 nm，而且光谱质量良好。另外，透射光谱图显示曝光时间在 120 s 内只有单个峰值出现，而且随着曝光时间延长，透射峰值有所下降，同时透射光谱中出现了次峰或多峰，光谱质量变差。这些实验结果表明，沿轴向施加一定张力刻写硫系光纤 Bragg 光栅，可以获得更高的光栅透射峰深度值，反射率显著提高，可高达 89.7%。

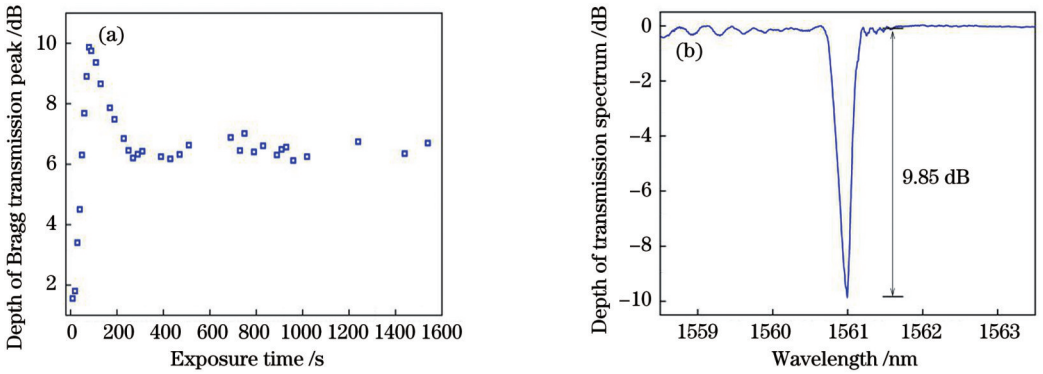

图 7 施加 0.196 N 张力刻写的 Bragg 光栅的特性。(a)Bragg 透射峰深度与曝光时间的关系；(b)曝光时间为 80 s 的 Bragg 光栅的透射光谱

Fig. 7 Characterization of written Bragg grating with tension of 0.196 N. (a) Dependence of the depth of Bragg transmission peak on exposure time; (b) transmission spectrum of Bragg grating with exposure time of 80 s

5 结 论

研究了 As_2S_3 硫系光纤在沿轴向施加张力下的光致折射率变化，结果表明，施加张力能显著提高光纤的光敏性。张力作用使得光致折射率变化 Δn 在第一快过程中的变化幅度减小，经历的时间明显缩短(在一定张力作用下可缩短至数十秒)；在第二慢过程中，光致折射率变化 Δn 加快朝正方向恢复，并在一定张力作用下出现正增长，且增长幅度随光照时间延长可高达 5.41×10^{-3}。

基于轴向张力能显著提高 As_2S_3 硫系光纤光敏性这一现象，采用改进型 Sagnac 干涉系统在拉锥形成的小直径单模 As_2S_3 硫系光纤上刻写 Bragg 光栅，在 70～110 s 的曝光时间内获得了质量良好的光栅透射谱，透射峰深度值平均达到了 9.46 dB，反射率最高可达 89.7%，明显优于未施加张力时的光栅性能。这些实验结果对于硫系玻璃光纤应用于力传感器、实现全光信息处理，以及改善和提高光敏性以制备高反射率的光纤光栅等硫系光子功能器件具有重要的应用价值。

参 考 文 献

[1] Eggleton B J, Luther-Davies B, Richardson K. Chalcogenide photonics[J]. Nature Photonics, 2011, 5(3): 141-148.

[2] Petersen C R, Lotz M B, Markos C, et al. Thermo-mechanical dynamics of nanoimprinting anti-reflective structures onto small-core mid-IR chalcogenide fibers[J]. Chinese Optics Letters, 2021, 19(3): 030603.

[3] Zhang B, Zeng P Y, Yang Z L, et al. On-chip chalcogenide microresonators with low-threshold parametric oscillation[J]. Photonics Research, 2021(7): 1272-1279.

[4] Serna S, Lin H T, Alonso-Ramos C, et al. Nonlinear optical properties of integrated GeSbS chalcogenide waveguides[J]. Photonics Research, 2018, 6(5): B37-B42.

[5] Alzaid M, Qasem A, Shaaban E R, et al. Extraction of thickness, linear and nonlinear optical parameters of $Ge_{20+x}Se_{80-x}$ thin films at normal and slightly inclined light for optoelectronic devices[J]. Optical Materials, 2020, 110: 110539.

[6] 刘启明，赵修建，干福熹. Ge-As-S 体系玻璃中光学二次谐波发生及其极化机理分析[J]. 物理学报，2000，49(9)：1726-1730.
Liu Q M, Zhao X J, Gan F X. Second harmonic generation in the system Ge-As-S and analysis of the poling mechanism[J]. Acta Physica Sinica, 2000, 49(9): 1726-1730.

[7] Zou L E, He P P, Chen B X, et al. Nonlinear optical properties of $As_{20}S_{80}$ system chalcogenide glass using Z-scan and its strip waveguide under bandgap light using the self-phase modulation[J]. AIP Advances, 2017, 7(2): 025003.

[8] Zhang Q, Zeng J H, Zhu L, et al. Temperature sensors based on multimode chalcogenide fibre Bragg gratings[J]. Journal of Modern Optics, 2018, 65(7): 830-836.

[9] Gao W Q, Li X, Wang P, et al. Investigation on sensing characteristics of fiber Bragg gratings based on soft glass fibers[J]. Optik, 2018, 156: 13-21.

[10] Yousefi E, Hatami M. A numerical method for pulse propagation in nonlinear fiber Bragg grating with ternary stability nature[J]. Optical Fiber Technology, 2020, 54: 102075.

[11] Yosia Y, Ping S. Double optical bistability and its application in nonlinear chalcogenide-fiber Bragg gratings[J]. Physica B: Condensed Matter, 2007, 394(2): 293-296.

[12] Scholtz L, Ladányi L, Müllerová J. Numerically analyzed spectral and temporal management of all-optical switching based on chalcogenide bistable fiber Bragg gratings[J]. Optical and Quantum Electronics, 2017, 49(2): 48.

[13] 张倩，张培晴，曾江辉，等. 中红外 $Ge_{20}As_{20}Se_{15}Te_{45}$ 硫系玻璃光纤光栅光开关[J]. 红外与激光工程，2017，46(7)：0720002.
Zhang Q, Zhang P Q, Zeng J H, et al. Mid-infrared fiber grating optical switch of $Ge_{20}As_{20}Se_{15}Te_{45}$ chalcogenide glass[J]. Infrared

and Laser Engineering, 2017, 46(7): 0720002.
[14] Behzadi B, Aliannezhadi M, Hossein-Zadeh M, et al. Design of a new family of narrow-linewidth mid-infrared lasers[J]. Journal of the Optical Society of America B, 2017, 34(12): 2501-2513.
[15] Wang J, Hou Y B, Zhang Q, et al. High-power, high signal-to-noise ratio single-frequency 1 μm Brillouin all-fiber laser[J]. Optics Express, 2015, 23(22): 28978-28984.
[16] Bernier M, Fortin V, El-Amraoui M, et al. 3.77 μm fiber laser based on cascaded Raman gain in a chalcogenide glass fiber[J]. Optics Letters, 2014, 39(7): 2052-2055.
[17] Kohoutek T, Hughes M A, Orava J, et al. Direct laser writing of relief diffraction gratings into a bulk chalcogenide glass[J]. Journal of the Optical Society of America B, 2012, 29(10): 2779-2786.
[18] Kaganovskii Y, Freilikher V, Rosenbluh M. Evolution of surface relief gratings in $As_{20}Se_{80}$ amorphous chalcogenide films under laser illumination[J]. Journal of Non-Crystalline Solids, 2022, 588: 121611.
[19] Butcher H L, Lee D, Brownsword R, et al. Ultrafast laser-inscribed mid-infrared transmission gratings in IG2: modelling and high-resolution spectral characterization[J]. Optics Express, 2017, 25(26): 33617-33628.
[20] Zou L E, Chen B X, Du L P, et al. Photo- and thermally induced changes in the refractive index and film thickness of amorphous As_2S_8 film[J]. Journal of Applied Physics, 2008, 103(12): 123523.
[21] Stronski A, Revutska L, Meshalkin A, et al. Structural properties of Ag-As-S chalcogenide glasses in phase separation region and their application in holographic grating recording[J]. Optical Materials, 2019, 94: 393-397.
[22] 潘磊, 宋宝安, 肖传富, 等. 两种 Ge-Sb-Se 薄膜的光学性质及微观结构[J]. 物理学报, 2020, 69(11): 114201.
Pan L, Song B A, Xiao C F, et al. Optical properties and microstructure of two Ge-Sb-Se thin films[J]. Acta Physica Sinica, 2020, 69(11): 114201.
[23] 邹林儿, 张泽, 傅继武, 等. 532 nm 光诱导下低损耗 As_2S_3 光纤纤芯的光敏性及其光阻断效应现象[J]. 中国激光, 2018, 45(12): 1206003.
Zou L E, Zhang Z, Fu J W, et al. Photosensitivity and optical stopping effect of low-loss As_2S_3 optical fiber core under 532 nm light irradiation[J]. Chinese Journal of Lasers, 2018, 45(12): 1206003.
[24] 邹林儿, 何盼盼, 傅继武, 等. +1/−1 相位掩模板和 532 nm 激光下低损耗 As_2S_3 硫系光纤布喇格光栅的制备[J]. 光子学报, 2017, 46(7): 0706001.
Zou L E, He P P, Fu J W, et al. Fabrication of Bragg gratings in low-loss As_2S_3 chalcogenide fibers using +1/−1 phase mask and 532 nm laser[J]. Acta Photonica Sinica, 2017, 46(7): 0706001.
[25] Brawley G A, Ta′eed V G, Bolger J A, et al. Strong photoinduced Bragg gratings in arsenic selenide optical fibre using transverse holographic method[J]. Electronics Letters, 2008, 44(14): 846-847.
[26] Ahmad R, Rochette M, Baker C. Fabrication of Bragg gratings in subwavelength diameter As_2Se_3 chalcogenide wires[J]. Optics Letters, 2011, 36(15): 2886-2888.
[27] Riant I, Haller F. Study of the photosensitivity at 193 nm and comparison with photosensitivity at 240 nm influence of fiber tension: type IIa aging[J]. Journal of Lightwave Technology, 1997, 15(8): 1464-1469.
[28] Miller G A. Decrease in photosensitivity of erbium-doped fiber under tension: implications for distributed feedback fiber lasers[J]. Journal of Lightwave Technology, 2018, 36(14): 3040-3045.
[29] Abdulhalim I, Gelbaor M, Klebanov M, et al. Photoinduced phenomena in nano-dimensional glassy As_2S_3 films[J]. Optical Materials Express, 2011, 1(7): 1192-1201.
[30] Abdulhalim I. Model for photoinduced defects and photorefractivity in optical fibers[J]. Applied Physics Letters, 1995, 66(24): 3248-3250.
[31] Wei Z X, Li H P, Zheng W, et al. Fabrication of tunable nonlinearly chirped fiber gratings using fiber Bragg grating[J]. Optics Communications, 2001, 187(4/5/6): 369-371.

Photosensitivity of As_2S_3 Chalcogenide Fiber with Axial Tension and Its Application in Writing Bragg Gratings

Zou Liner*, Shang Lei, Yang Xifei, Shen Yun

School of Physics and Materials Science, Nanchang University, Nanchang 330031, *Jiangxi, China*

Abstract

Objective Among the many photonic devices, the Bragg grating of chalcogenide glass fibers is important. As a linear device, it can be applied to infrared sensors. In nonlinear optical applications, it can achieve all-optical signal processing. In addition, it is necessary to apply Bragg grating with high reflectivity to obtain efficient integrated chalcogenide glass fiber lasers, such as the distributed feedback Brillouin lasers. For chalcogenide glass fibers, it is complex to write Bragg gratings, mainly because the cladding and core components of chalcogenide glass fibers are similar; thus, both show photosensitivity, resulting in the weak photosensitivity of the fiber core. In our previous study, near-bandgap light close to the absorption edge of the material was selected to irradiate the chalcogenide glass fiber. The fiber core showed high photosensitivity, which solved the weak photosensitivity caused by sub-bandgap light far from the absorption edge of the material. However, when the fiber is used to write a Bragg grating, the depth of the grating transmission peak is not extended and cannot satisfy the actual usage requirements. This requires methods to further improve the photosensitivity of chalcogenide fibers. Therefore, this study extensively investigated the photosensitivity of chalcogenide optical fibers in tension applied in the axial direction to improve the photosensitivity of chalcogenide fibers and provide a new approach to writing gratings with high reflectivity. The findings provide new ideas and approaches for preparing chalcogenide grating photonic devices and will promote the development of chalcogenide photonics.

Methods The photosensitivity of chalcogenide optical fibers was determined by measuring the change in the refractive index of the fiber core based on the Fabry-Perot (FP) etalon principle. In this experimental device, an optical fiber clamp with a slider was designed to apply tension, and a continuous dual-frequency Nd∶YAG laser with a working wavelength of 532 nm was used as the illumination source. After the laser beam was expanded using the beam-expansion system, it was focused onto the sample surface through a

cylindrical lens to form a light spot with a height of approximately 1.1 mm and width of approximately 5 mm. The As_2S_3 optical fiber was cut using an ultrasonic cutter to produce an FP etalon of approximately 15 mm in length.

An improved Sagnac interference system, constructed using the same Nd∶YAG laser and a phase mask with a +1/−1 diffraction order, was used to form interference fringe patterns for writing the fiber Bragg gratings. In this system, the optical path of the Sagnac interference system was optimized to ensure that the two Gaussian light spots have improved coincidence and obtain interference fringes with increased contrast.

Results and Discussions The experimental results show a significant difference in photosensitivity between the presence and absence of tension (Figs. 2 and 3). By applying tension, the photorefractive index change in the first fast process presents a decrease in the amplitude of the negative change of the refractive index, and the duration of the first fast process shortens. During the second slow process under tension, the recovery time of the photorefractive index change in the positive direction also shortens, and the change in the photorefractive index slowly recovers with the extension of the illumination time and can reach 10^{-3} orders of magnitude. Under the same tension, during the first fast process of photorefractive index change, its duration is significantly shortened with an increase in light power [Figs. 2(b) and 3(b)], which can be shortened to tens of seconds. During the second slow process, the recovery of the photorefractive index change is also accelerated, and the change in the photorefractive index shows a positive increase under a specific tension, which can reach 5.41×10^{-3}. Under the same light power, the duration of the first fast process is significantly shortened with an increasing axial tension, whereas the negative change amplitude of the photorefractive index change decreases. In the second slow process, the change in the photorefractive index recovers faster under larger tension (Fig. 4).

The dynamic characteristics of Bragg grating written on a small-diameter fiber sample under a tension of 0.196 N were investigated. Without applying axial tension, the maximum depth of the transmission peak of the engraved Bragg grating was approximately 6.65 dB, and the reflectivity is approximately 78% (Fig. 6). However, when a tension of 0.196 N is applied, the transmission peak of the Bragg grating can reach 9.85 dB, the reflectivity increases to 89.7%, and the grating bandwidth is approximately 0.48 nm (Fig. 7). During the exposure time of 70–110 s under tension, the average depth of the transmission peak of the grating reaches 9.46 dB, the average reflectivity reaches 88.6%, and a good-quality grating spectrum can be obtained (Fig. 7).

Conclusions In this study, the characteristics of the photorefractive index change of an As_2S_3 chalcogenide optical fiber under axial tension were experimentally investigated. The experimental results show that there is a significant difference in the photosensitivity with and without tension. By applying tension, the negative change amplitude of the photorefractive index change in the first fast process can reduce, and the duration of the first fast process shortens significantly, which can be shortened to tens of seconds under a particular tension. In the second slow process, under tension, the recovery time of the photorefractive index change in the positive direction also shortens, and the photorefractive index change shows a positive increase under a certain tension, which can reach 5.41×10^{-3}. On this basis, the As_2S_3 chalcogenide fiber Bragg grating was written based on the remarkable photosensitivity caused by the application of tension. The grating spectrum shows that within 70–110 s short exposure time, the average depth of transmission peak of the grating reaches 9.46 dB, the maximum depth of peak is 9.85 dB, the maximum reflectivity reaches 89.7%, and the grating spectrum quality is good. These experimental results are crucial in applying chalcogenide glass fibers in the near-middle infrared field as force sensors, achieving all-optical signal processing, and improving photosensitivity for preparing fiber gratings with high reflectivity.

Key words fiber optics; chalcogenide glass fiber; tension; photosensitivity; fiber grating